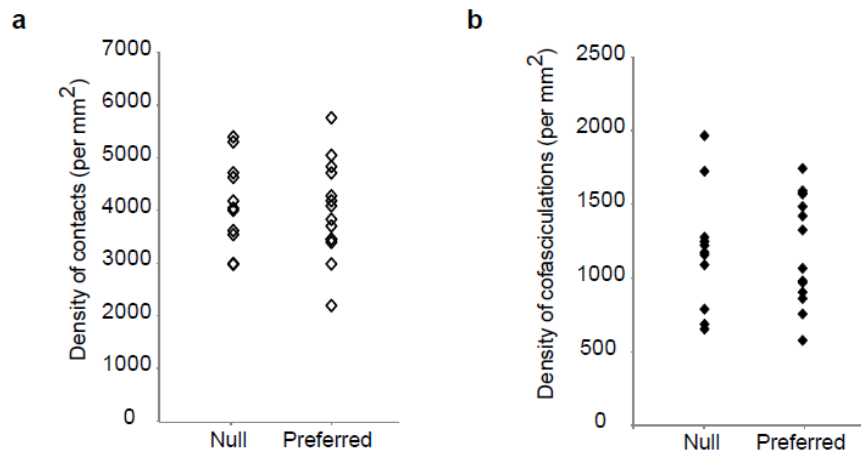


## Supplementary Figure 1

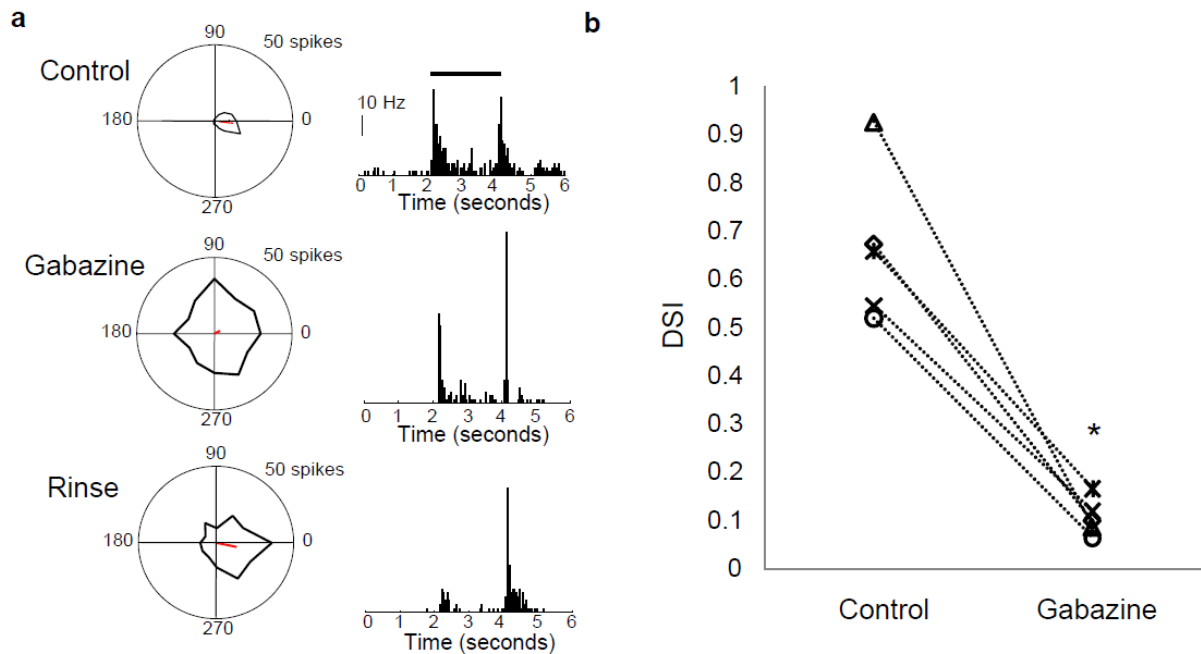


Supplementary Figure 1. Entire processes of SACs located on the null or preferred side of nDSGCs show a similar density of contacts and cofasciculations with nDSGCs dendrites. In Figure 3 of the paper, we restricted this analysis to the outer third of SAC processes.

a. Summary plot of the density of contacts between DSGCs and SACs from the null or preferred side from P14 to 48.

b. Summary plot of the density of cofasciculations between SACs and DSGCs from the same pairs as in a. No significant difference was found between the null and preferred side groups in a or b.  $p > 0.7$ , t-test.

## Supplementary Figure 2

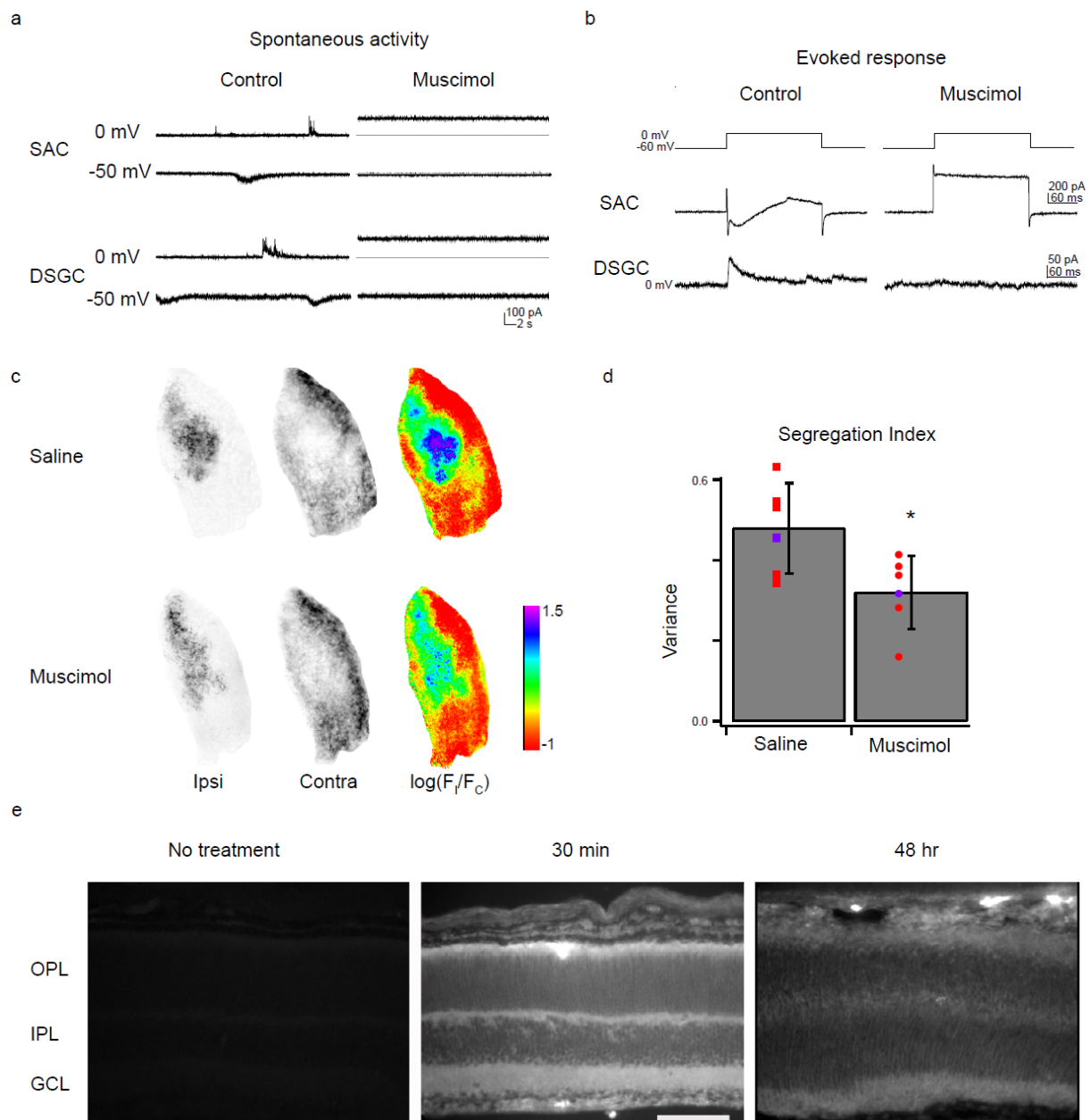


Supplementary Figure 2. Acute GABA-A receptor blockade abolishes direction selectivity in On-Off nDSGCs.

a. Light responses of a GFP+ neuron from a P14 *Drd4-GFP* mouse before, during and after application of the GABA-A receptor antagonist gabazine (1.25  $\mu$ M). Spike tuning curves to drifting gratings are shown in the left panel, and spike density histograms of the same cells to 100  $\mu$ m stationary spots in the right panel. Black bar indicates the time during which a white spot was presented.

b. Direction selective index (DSI) from five GFP+ neurons before and during gabazine application. \* $p < 0.001$ , paired t-test.

## Supplementary Figure 3



Supplementary Figure 3. Application of muscimol effectively blocks retinal activity and disrupts eye-specific segregation.

a. Example traces from whole-cell voltage-clamp recordings of inhibitory (upper traces,  $V_H=0$  mV) and excitatory (lower traces,  $V_H=-50$  mV) currents from a P8 SAC and a P8 nDSGC in ACSF (Control, left) or ACSF containing 100  $\mu$ M muscimol (right). Deflections from baseline correspond to compound synaptic currents associated with retinal waves. Note, at depolarized

potentials, application of muscimol activated a tonic current, which was measured as a change in the baseline holding current<sup>1</sup>.

b. Paired whole-cell voltage-clamp recordings of inhibitory currents in a P8 nDSGC (lower traces) evoked by depolarization of a SAC from -60 mV to 0 mV (upper traces) in drug-free ACSF (Control, left) or in ACSF containing 100  $\mu$ M muscimol (right). Recording conditions were the same as in Figure 1 of the paper.

c. Fluorescence images of dorsal Lateral Geniculate Nuclei (dLGN) sections ipsilateral to the eye treated with either saline (top) or muscimol (bottom). Left, fluorescence of Alexa 594-labeled retinogeniculate axons from the treated eye; Middle, fluorescence of Alexa 488-labeled axons from the untreated eye; Right, pseudocolor images based on the logarithm of the intensity ratio, ( $R = \log(F_I/F_C)$ ) for each pixel, a parameter that reflects the extent of segregation<sup>2</sup>.

d. Summary of the variance of the distribution of the R-values for all the pixels in the images in part c. The broader the distribution of R-values is for a given LGN, the greater the extent of segregation (see Supplementary Methods below). Points are individual brains and error bars are standard deviation. The purple data points represent examples shown in c. \* $p = 0.02$ , t-test.

e. Fluorescent images of retinas from C57B/6 mice receiving no treatment (left, P6), an intraocular injection of fluorescently-labeled muscimol at 30 min (middle, P6) and 48 hours (right, P8) prior to imaging. The exposure time for “No treatment” and “48 hours” was 500 ms, for “30 min” was 50 ms. Scale bar: 100  $\mu$ m.

#### Supplementary Discussion and Methods for this Figure:

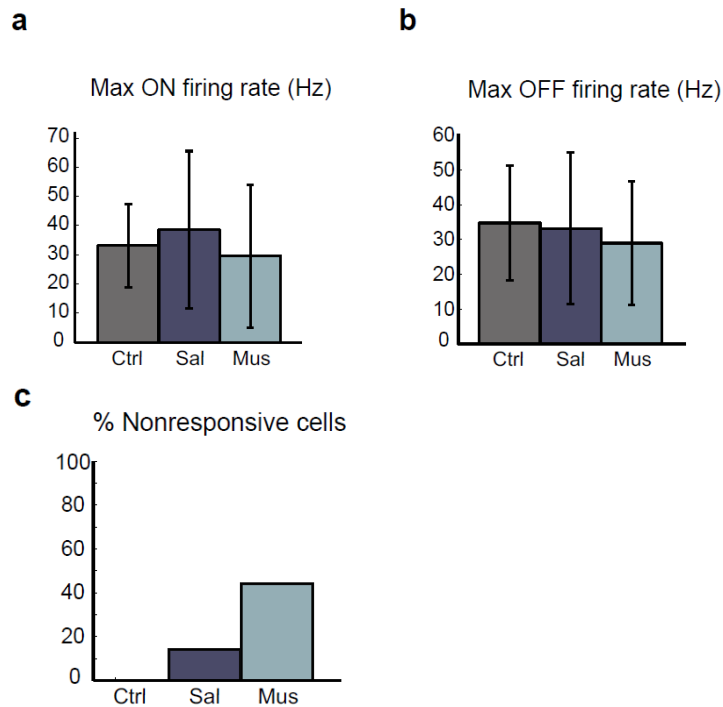
As an independent measure of the effectiveness of muscimol at blocking retinal activity, we monitored the effect of monocular muscimol injections on the eye-specific segregation of retinogeniculate projections<sup>3</sup>. Though the bulk of eye-specific segregation is complete by P8, there is a small amount of additional segregation that occurs between P8 and P14<sup>4, 5</sup>. To monitor the effects of activity blockade during the second postnatal week, when direction selective circuits emerge, we performed intraocular injections of muscimol at P6, P8, P10 and P12, and computed the segregation index by a method that objectively quantifies the extent of segregation<sup>2</sup>. A significant reduction in eye-specific segregation was found in muscimol-treated animals. For a subset of experiments, eye-specific segregation was analyzed in the same brains of animals from which retinas were used for recordings (Figure 4 of main text). However, we found no correlation between the value of the directional tuning and the extent of segregation (data not shown). These findings indicate that intraocular injection of muscimol during the second postnatal week is an effective means of blocking activity *in vivo*.

Animals were anesthetized with 3.5% isoflurane/2% O<sub>2</sub>. The eyelid was then opened with fine forceps to expose the eye, and 0.1-1  $\mu$ l of Alexa-488 or Alexa-594 conjugated  $\beta$ -cholera toxin was injected using a fine glass micropipette with a picospritzer (World Precision Instruments, Sarasota, FL) generating 20 psi, 3 ms long positive pressure. The cholera toxin was then allowed to transport for 24 hours, which was sufficient time for clear labeling of axons and terminals. Brains were removed, immersion fixed in 4% paraformaldehyde (24 hours), cryo-protected in 30% sucrose (18 hour) and sectioned coronally (100  $\mu$ m) on a Vibratome.

Images were analyzed as described previously<sup>2</sup>. Briefly, eight-bit tagged image file format images were acquired for Alexa488- or 594-labeled sections of the LGN with a CCD camera (Optronics, Goleta, CA) attached to an upright microscope (Zeiss Axioscope 2; Thornwood, NY)

with a 10X objective (numerical aperture, 0.45). The three sections that contained the largest ipsilateral projection, corresponding to the central third of the LGN, were selected, and all analysis was performed on these sections using the side of the brain that was ipsilateral to the muscimol injection (Alexa594-labeled ipsilateral/Alexa488-labeled contralateral projection). Background fluorescence was subtracted using a rolling ball filter (NIH Image) and the grayscale was renormalized so that the range of grayscale values was from 0 to 256. IgorPro Software (Wavemetrics, Lake Oswego, OR) was used to perform a segregation analysis. For each pixel, we computed the logarithm of the intensity ratio,  $R = \log_{10}(F_I/F_C)$ , where  $F_I$  is the ipsilateral channel fluorescence intensity and  $F_C$  is the contralateral channel fluorescence intensity. We then calculated the variance of the distribution of R values for each section, which was used to compare the width of the distributions across animals. A higher variance is indicative of a wider distribution of R-values, which is in turn indicative of more contra- and ipsi-dominant pixels, and therefore more segregation.

Intraocular injection of fluorescently labeled muscimol (BODIPY TMR-X muscimol, Invitrogen) was performed according to the same protocol for unlabeled muscimol (See Methods Summary in the paper). Retinas from the injected eyes were dissected at 30 min or 48 hours after injection, fixed in 4% paraformaldehyde (24 hours), and sectioned (20  $\mu\text{m}$ ) on a cryostat. Fluorescent images were taken with a CCD camera (Optronics).

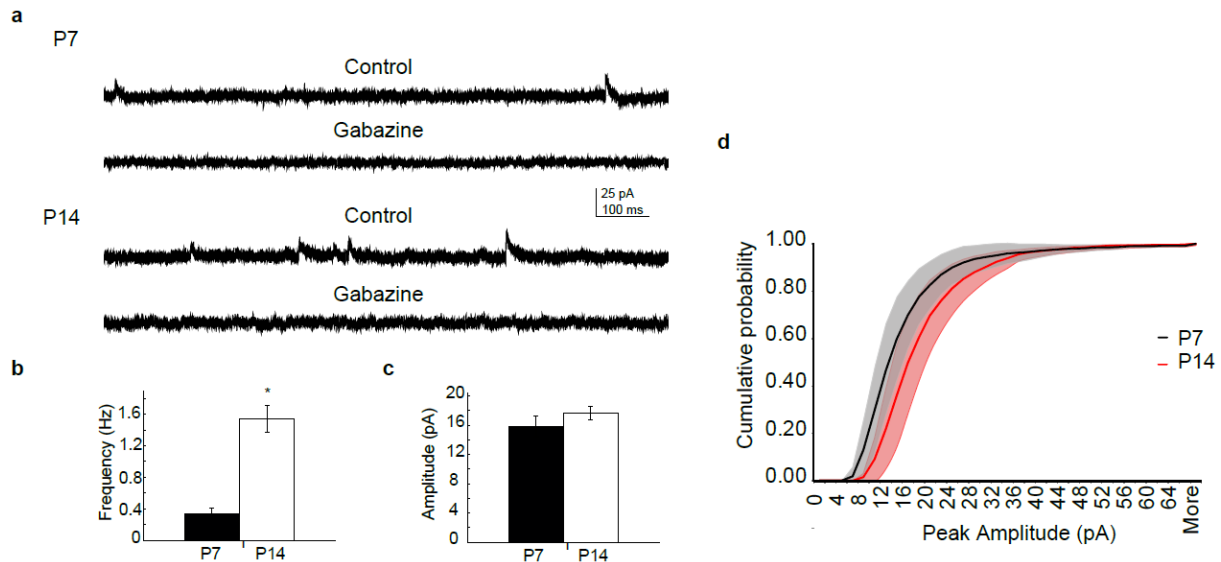
**Supplementary Figure 4**

Supplementary Figure 4. Muscimol-treated nDSGCs exhibit On and Off responses but have a higher percentage of cells that do not respond to drifting gratings.

a and b. Summary plots of the maximum firing rate during the On (**a**) and Off (**b**) responses to 100  $\mu\text{m}$  stationary spots (10 repetitions, 50 ms bins) for uninjected retinas (Ctrl), retinas receiving repeated injections of saline (Sal) or muscimol (Mus). Values represent mean  $\pm$  standard deviation.

c. Summary plot of the percentage of cells not responsive to drifting gratings but exhibiting normal On-Off responses to stationary spots.

## Supplementary Figure 5



Supplementary Figure 5. Spontaneous GABAergic IPSCs of nDSGCs show a significant increase in the frequency from P7 to P14.

a. Whole-cell voltage-clamp recordings ( $V_H=0$  mV) of spontaneous IPSCs from GFP+ neurons in P7 (top) and P14 (bottom) *Drd4-GFP* mice in the absence (top) and presence (bottom) of gabazine (5 $\mu$ M). Recordings were in the presence of 8  $\mu$ M DH $\beta$ E, 50  $\mu$ M APV, 20  $\mu$ M NBQX and 1  $\mu$ M TTX.

b and c. Summary plots of the frequency (b) and peak amplitude (c) of the spontaneous IPSCs of the nDSGCs at P7 and P14. P7:  $n = 14$  cells; P14:  $n = 11$  cells. Error bars represent standard error. \* $p < 0.0001$ , t-test.

d. Cumulative distribution curves of the spontaneous IPSC peak amplitude for nDSGCs at P7 and P14. Shaded areas indicate standard deviation.

Supplementary Discussion for this Figure:

The significant increase in IPSC frequency is consistent with the hypothesis that the null-side pairs develop more functional GABAergic synapses than the preferred side pairs. However, analysis of spontaneous synaptic events is complicated by the fact that the inputs are from all synapses onto a given DSGC and there is no way to distinguish inputs from preferred or null side starburst cells. Hence the modest change in synaptic strength may represent strengthening of the existing null-side synapses. Conclusive statements about whether changes in unitary conductance are due to changes in number and/or strength will require an extensive characterization of the quantal properties of the synapse during development.

### Supplementary References

1. Wang, C. T. et al. GABA(A) receptor-mediated signaling alters the structure of spontaneous activity in the developing retina. *J Neurosci* 27, 9130-40 (2007).
2. Torborg, C. L. & Feller, M. B. Unbiased analysis of bulk axonal segregation patterns. *J Neurosci Methods* 135, 17-26 (2004).
3. Huberman, A. D., Feller, M. B. & Chapman, B. Mechanisms underlying development of visual maps and receptive fields. *Annu Rev Neurosci* 31, 479-509 (2008).
4. Torborg, C. L. & Feller, M. B. Spontaneous patterned retinal activity and the refinement of retinal projections. *Prog Neurobiol* 76, 213-35 (2005).
5. Guido, W. Refinement of the retinogeniculate pathway. *J Physiol* 586, 4357-62 (2008).